THE JOURNAL OF PHYSICAL CHEMISTRY B

Article

pubs.acs.org/JPCB

Molecular Dynamics Simulations of CO_2 and Brine Interfacial Tension at High Temperatures and Pressures

Xuesong Li, Daniel A. Ross, J. P. Martin Trusler, Geoffrey C. Maitland, and Edo S. Boek*

Qatar Carbonates and Carbon Storage Research Centre (QCCSRC), Department of Chemical Engineering, Imperial College London, South Kensington Campus, London SW7 2AZ, United Kingdom

ABSTRACT: Molecular dynamics simulations have been performed to study the interfacial tension of CO_2 and brine for a range of temperatures between 303 and 393 K and pressures from 2 to 50 MPa. The ions involved in this study are Na^+, Ca^{2+}, and Cl^-. The results indicate that the interfacial tension decreases with increasing pressure under any temperature condition but increases linearly with the molality of the salt solution. The density profiles calculated from the MD simulation results also indicate a positive excess of CO_2 and a negative excess of ions at the interface. The charge of the ions was found to have a larger influence than their size on the interfacial tension, a result that consistent with experimental findings.

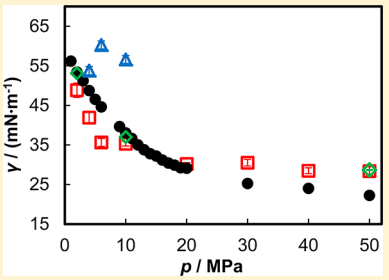

1. INTRODUCTION

Many oil reservoirs typically comprise porous rocks containing oil and gas at high temperatures and pressures deep underground. After primary and secondary production, as much as 50% of the original oil in place (OOIP) may be left behind in the reservoir.[1] The interfacial tension (IFT) is considered to be an important factor that may render as much as 30% of the OOIP unrecoverable by solution gas drive or water flooding alone. Recovery may be improved by injecting carbon dioxide to displace and dissolve some of the remaining oil.[2] In general, it has been found that such tertiary processes can enhance oil recovery by 8 to 16% of the OOIP.[3] Interfacial phenomena between hydrocarbon-, water- and CO_2-rich phases clearly play a very important role in determining the effectiveness of CO_2-enhanced oil recovery (CO_2-EOR).

In the CO_2-EOR processes, both the relative permeabilities of the formation to oil and CO_2 and the residual oil saturation can be related to the oil−CO_2 and brine−CO_2 IFTs through a dimensionless number that compares the capillary and viscous forces in horizontal displacement processes or the capillary and buoyancy forces in gravity drainage processes.[4−6] Although there have been some studies of the effects of IFT in oil−CO_2 and water−CO_2 systems on the relative permeabilities in the CO_2 flooding process,[7−11] there are insufficient data available in the literature for analyzing the effects of IFT between oil, CO_2, and brine on the CO_2-EOR process. It has been found that the viscosity of an oil−brine system is significantly reduced when CO_2 is injected into an oil reservoir at a high reservoir pressure.[12,13] The reduced IFT alters the balance between viscous and capillary forces and thus lowers the residual oil saturation. Finally, the low viscosity of supercritical CO_2 puts severe limits on the efficiency of both carbon storage and CO_2-EOR as the sweep efficiency is often reduced due to channelling and fingering effects, associated with reservoir heterogeneity.[14] Therefore, it is of fundamental and practical importance to study the detailed effects of the viscous and capillary forces on various CO_2 flooding processes.

The study of interfacial properties between carbon dioxide and the fluids and minerals present in oil reservoirs and deep saline aquifers is fundamental to a scientific understanding of geological carbon storage. The technologies and practices that have been developed for CO_2-EOR have to some extent applicability in carbon storage processes.

In previous work we explored the IFT of CO_2 and water/brines as a function of temperature and pressure over a wide range of the salinity of brine,[15,16] and it was found that IFT increases linearly with molality. Furthermore, at constant temperature and pressure, the IFT is the same function of the positive charge molality for all investigated salts, that is, mixtures of NaCl and KCl, $CaCl_2$, $MgCl_2$, and Na_2SO_4. In this article, we use MD simulations to validate the hypothesis in our previous experimental paper of CO_2 and brine systems. We briefly explain this hypothesis. Also, we will use MD simulations to obtain deeper insight into the reasons for different dependence of IFT on temperature, pressure, and the salinity of brines.

Molecular dynamics simulations of pure water and CO_2 system have been carried out by various authors.[17−21] The surface tension of water has been investigated by Chen et al.[22] with different water models. The IFT of pure water and CO_2 system was studied by Nielsen et al.[23] Zhao et al.[38] analyzed the effect of salinity on the interfacial structure in CO_2/brine solutions. Here we extend these studies and include explicit comparison with recent experimental observations.[15,16]

Received: October 1, 2012
Revised: March 26, 2013
Published: March 28, 2013

   dx.doi.org/10.1021/jp309730m | J. Phys. Chem. B 2013, 117, 5647−5652

2. METHODS

2.1. Force-Field Selection. Two typical water models, SPC/E[24] and TIP4P,[25] are investigated together with the EPM2 model for CO_2.[18,20,21,26,27] The SPC/E force field was chosen because of its ability to reproduce water self-diffusion, dissolved CO_2 solvent structure,[17] orthobaric density,[28] static dielectric constant,[29] and PVT properties up to high pressures[30] and because it provides one of the best predictions of the vapor−liquid IFT of water.[22,31] Despite some early, now controversial results indicating that the SPC/E model accurately reproduces the water vapor−liquid IFT,[28] most simulations of water vapor−liquid IFT using the SPC/E force field underestimate the vapor−liquid by up to 10 $mN{\cdot}m^{-1}$.[22,31] Indeed, most commonly used fixed-charge water models significantly underestimate the surface tension of liquid water. The TIP4P water model has been shown to provide a better estimate of water vapor−liquid IFT,[31] so this water model was also selected for comparison. The EPM2 model was chosen for carbon dioxide because of its good prediction of the liquid−vapor coexistence curve.[26] The EPM2 CO_2 molecules were treated in the simulation by adding two dummy sites to the molecules carrying the total mass of the molecule, while the carbon and oxygen atoms have zero mass but carry the 6−12 Lennard-Jones parameters and atoms charges. The positions of the mass sites have been chosen to preserve the moment of inertia tensor of the original EPM2 model.[39] The 6−12 Lennard-Jones parameters of the ions explored in this study are obtained from the OPLS-AA all-atom force field.[32] These parameters together with EPM2 CO_2 used in this study are summarized in Table 1.

Table 1. Lennard-Jones Parameters of Atoms

atoms	σ (nm)	ε ($kJ{\cdot}mol^{-1}$)	charge (e)	mass (g/mol)
Ions				
Na^+	0.333045	0.011598	1.000	22.98977
Ca^{2+}	0.241203	1.88136	2.000	40.08000
Cl^-	0.441724	0.492833	−1.000	35.45300
EPM2 CO_2				
D1	0	0	0	22.00475
D2	0	0	0	22.00475
C	0.2757	0.23379	0.6512	0
O	0.3033	0.66912	−0.3256	0

2.2. Simulation Methods. This study was performed with the GROMACS 4.5.4 MD simulation code[33] using periodically boundary conditions. For the NaCl(aq) and CO_2 system, two different brine salinities were studied, which are 1.73 and 3.46 $mol{\cdot}kg^{-1}$. For the $CaCl_2$(aq) and CO_2 system, we have the same number of water, CO_2, and Cl^- molecules as in the NaCl(aq) and CO_2 systems.

Before carrying out the systematic study with a large range of temperature and pressure variation, the system size was optimized by comparing simulation results for different system sizes, containing different numbers of water molecules under certain temperature and pressure conditions. The number of CO_2 molecules was always adjusted according to the pressures. We found that for high pressures the systems containing 1024 and 4096 water molecular gave similar results. For low pressures, the larger system seems to give better results. The smallest system containing 512 water molecules yields different simulation results due to the small amount of water molecular in the system. In Figure 1, we present the IFT of water and CO_2 as a function of pressure.

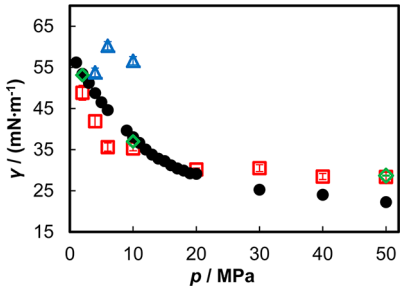

Figure 1. Pressure dependence of interfacial tension of SPC/E-EPM2 system with different particle numbers at T = 373 K. Symbols (number of water molecules/number of CO_2 molecules): blue △, 512/256; red □, 1024/512; green ◇, 4096/2048; ●, ref 35.

The simulation was initialized by placing all of the particles in a control box for NPT simulation. After reaching a dynamic equilibrium, the dimensions of the box were fixed and a further 10 ns NVT simulation was performed, from which the final results were obtained.

During the simulation, the Nose−Hoover extended ensemble was used for temperature coupling. The Parrinello−Rahman method was used for pressure coupling in the NPT simulation. In this scheme, the simulation box vectors are subject to an equation of motion and no instantaneous scaling takes place. The pressure coupling is governed by the time constant t_p (ps) associated with the period of pressure fluctuations at equilibrium. An anisotropic pressure coupling type was used, and only the z dimension oscillated in the simulation. Strictly speaking, therefore, we are working in the constant ($NP_{zz}T$) ensemble. To avoid large oscillations, which may occur especially at a pressure near the critical pressure of CO_2, the initial volume of the box was very carefully set with reference fluid densities.[34] Meanwhile, a total compressibility of the system was given by interpolating the compressibility of each phase from ref 34.

For both NPT and NVT simulations, the long-range Coulomb intermolecular forces are treated using the particle-mesh Ewald (PME) technique. Also, we applied long-range dispersion corrections for energy and pressure.

2.3. Interfacial Tension. During the NVT simulation, the IFT was determined by the principal components of the MD simulation cell stress tensor, as detailed in Harries et al.[36] (and Matsumoto and Kataoka, 1988; Kuznetsova and Kvamme, 2002):

$$\gamma = \frac{1}{2}L_Z\left[P_{ZZ} - \frac{1}{2}(P_{xx} + P_{yy})\right] \quad (1)$$

where L_Z (nm) is the box length in the Z direction and $P_{\alpha\alpha}$ is the $\alpha\alpha$ component of the pressure tensor. A sketch of simulation is shown in Figure 2, where the z direction is normal to the two brine and CO_2 interfaces.

3. RESULTS AND DISCUSSION

In the following sections, we will present our results on density profile and surface excess, pressure and temperature dependence, brine salinity dependence, and solubility.

3.1. Density Profile and Surface Excess. In Figure 3, we present a snapshot of the simulation domain of the brine and

dx.doi.org/10.1021/jp309730m | J. Phys. Chem. B 2013, 117, 5647−5652

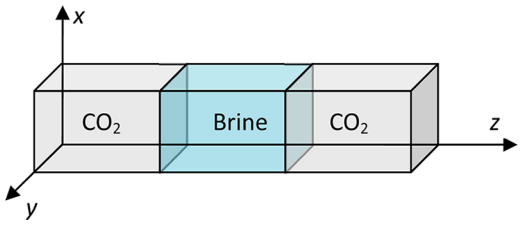

Figure 2. Sketch of simulation domain configuration.

CO_2 system at 373 K and 2 MPa. 128 Ca^{2+}, 256 Cl^-, 4096 SPC/E water, and 512 EPM2 CO_2 molecules are within the control box. The system has dimensions of 5 × 5 × 51.73 nm in *x*, *y*, and *z* directions, respectively. The condensed phase in the center is brine, and the less dense phase is CO_2-rich gas.

A detailed density profile of the interface is calculated from the GROMACS simulations, as shown in Figure 4. This density profile yields a 2 nm interface. A positive excess of CO_2 can be observed together with a negative excess of ions. Similar phenomena were found for NaCl(aq) and CO_2 systems at different temperatures and pressures.

The total number of moles of water, CO_2, and ions remains constant in the bulk phases but vary at the surface, as shown in Figure 4. The surface excess represents the difference between the total number of moles of the *i*th component in the system and in a particular phase, CO_2 or brine, and is represented by:

$$\Gamma_i = \frac{n_i^{\text{total}} - n_i^{\text{CO}_2} - n_i^{\text{brine}}}{A} \quad (2)$$

where Γ_i is the surface excess of the *i*th component, *n* is the number of moles, CO_2 and brine are the phases, and *A* is the area of the dividing surface. Γ represents the excess of solute per unit area of the surface over the bulk concentration extrapolated to the interface, calculated directly from the density profile. From the density profiles in Figure 4, we observe that Γ_{CO_2} is a positive term that has a value of 8.47 × 10^{-4} mol·m^{-2} but Γ_{ion} is a negative term which is around −5.92 × 10^{-4} mol·m^{-2}.

3.2. Pressure and Temperature Dependence. We observe that both water models, TIP4P and SPC/E, qualitatively predict the IFT values found experimentally, as shown in Figures 5−7, respectively. The IFT decreases with increasing pressure, keeping the temperature and brine salinity constant. However, comparing Figure 5 with Figure 6, using the same number of molecules and the same simulation control parameters, it can be seen that the SPC/E water model gives results that agree better with experiment.

Our previously published experimental results of the IFT at high pressures demonstrated that NaCl and $CaCl_2$ brine solutions with the same positive charge concentration give similar IFT results at different pressures at *T* = 373 K. The same behavior was observed at other temperatures as well.[15,16] Figure 5 shows that the MD simulation results for the IFT of brine and CO_2 is consistent with this dependence on positive charge concentration.

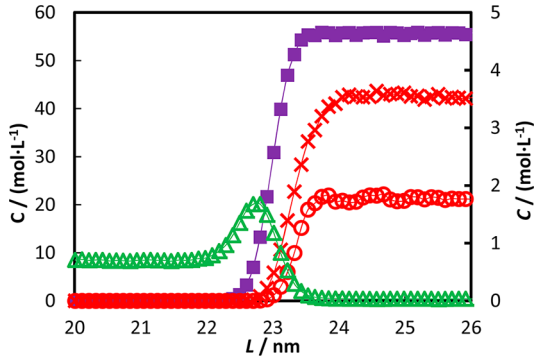

Figure 4. Density profile of brine−CO_2 interface simulation equilibrated at *T* = 373 K, *p* = 2 MPa. The molar concentration of water is scaled at the left, and ions and CO_2 are scaled at the right. Particle numbers: Ca^{2+}, 128; Cl^-, 256; water SPC/E, 4096; and CO_2 EPM2, 512. Symbols: purple ■, water; red ×, Cl^-; red ○, Ca^{2+}; and green △, CO_2.

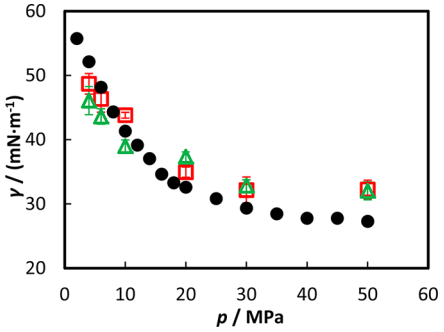

Figure 5. Pressure dependence of interfacial tension of brine−CO_2 system at *T* = 373 K. Particle numbers: Na^+, 16; Ca^{2+}, 8; Cl^-,16; water SPC/E, 1024; and CO_2 EPM2, 512. Symbols: △, MD of NaCl(aq) and CO_2; □, MD of $CaCl_2$(aq) and CO_2; and ●, ref 15.

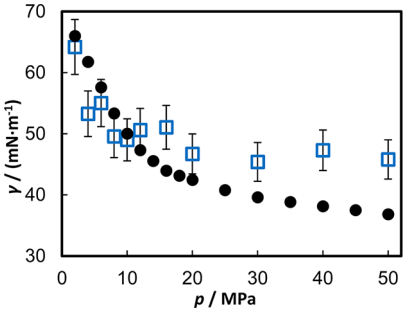

Figure 6. Pressure dependence of interfacial tension between NaCl(aq) and CO_2 at *T* = 373 K. Particle numbers: Na^+, 128; Cl^-, 128; water TIP4P, 1024; and CO_2 EPM2, 512. Symbols: □, MD of NaCl(aq) and CO_2; ●, ref 15.

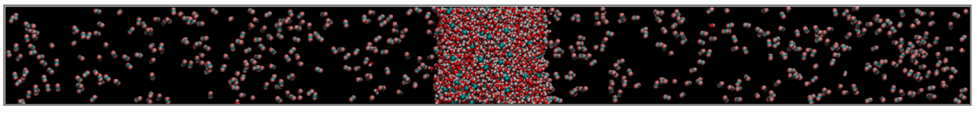

Figure 3. Snapshot of the simulation domain of a brine−CO_2 system equilibrated at *m* = 3.46 mol·kg^{-1}, *T* = 373 K, and *p* = 2 MPa. Particle numbers: Ca^{2+}, 128; Cl^-, 256; water SPC/E, 4096; and CO_2 EPM2, 512.

dx.doi.org/10.1021/jp309730m | J. Phys. Chem. B 2013, 117, 5647−5652

From Figures 5−7, we generally observe good qualitative agreement between experimental and simulation data. However, quantitatively the simulation data start to deviate from the experiment with pressure increasing. A possible cause for this discrepancy could be the brine density in the simulation. One may assume that the calculation of the IFT is strongly affected by the density of the system, in the sense that a higher density would produce a higher IFT. To address this point, we have calculated the pressure dependence of the brine density. In Figure 8, we present the densities for NaCl(aq) and CaCl2(aq) brines using SPC/E water in comparison with a recent experimental correlation.[40] In Figure 9, we show the densities of NaCl(aq) brine using TIP4P water as a function of pressure in comparison with experiment.[40] We observe that the calculated density of the brines increases with increasing pressure, following the same trend as the experiment. The calculated densities are consistently less than 2% (SPC/E) and 3% (TIP4P) smaller for all pressures considered. In our view, these results for the calculated density in comparison with the experimental density are acceptable. However, these results do not explain the observed deviation for the surface tension at high pressures only. We suggest that this could be due to other simulation parameters, such as system size. We are currently further investigating finite size effects and will report on this in the near future.

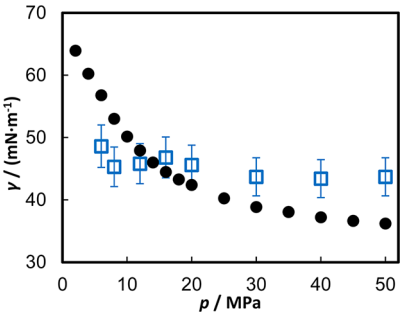

Figure 7. Pressure dependence of interfacial tension between NaCl(aq) and CO_2 at T = 393 K. Particle numbers: Na^+, 128; Cl^-, 128; water TIP4P, 1024; and CO_2 EPM2, 512. Symbols: □, MD of NaCl(aq) and CO_2; ●, ref 15.

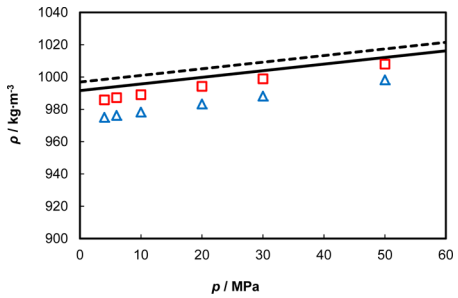

Figure 8. Pressure dependence of brine density at T = 373 K for SPC/E water. Particle numbers: Na^+, 64; Ca^{2+}, 32; Cl^-, 64; and water SPC/E, 1024. Symbols: △, MD of NaCl(aq); □, MD of $CaCl_2$(aq); [solid line], NaCl(aq) reference; and [dashed line], $CaCl_2$(aq) ref 40.

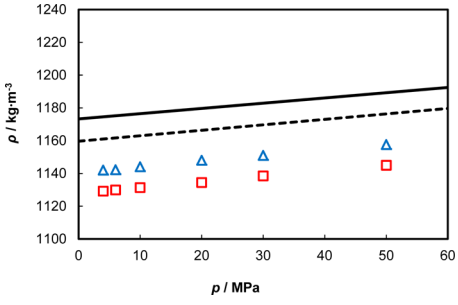

Figure 9. Pressure dependence of NaCl(aq) brine density at T = 373 and 393 K for TIP4P water. Particle numbers: Na^+, 512; Cl^-, 512; and water TIP4P, 4096. Symbols: △, MD at 373K; □, MD at 393 K; [solid line], 373 K reference; and [dashed line], 393 K ref 40.

3.3. Brine Salinity Dependence. Figures 10 and 11 show the IFT dependence on brine salinity under different pressures

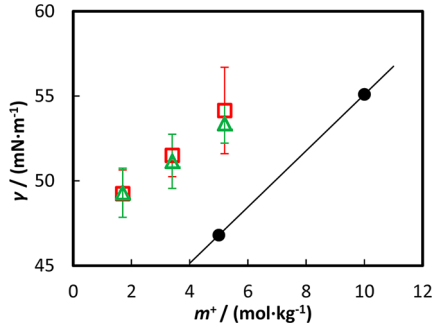

Figure 10. Interfacial tension dependence on brine salinity at T = 373 K, p = 10 MPa. Particle numbers: water TIP4P, 1024; CO_2 EPM2, 512. Symbols: △, MD of NaCl(aq) and CO_2; □, MD of $CaCl_2$(aq) and CO_2; and ●, ref 15.

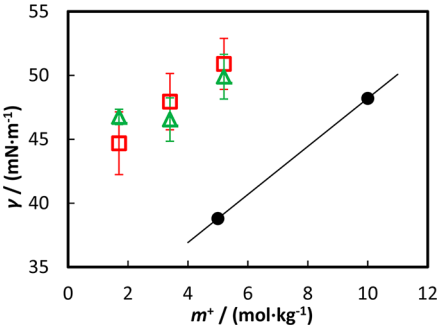

Figure 11. Interfacial tension dependence on brine salinity at T = 373 K, p = 20 MPa. Particle numbers: water TIP4P, 1024; CO_2 EPM2, 512. Symbols: △, MD of NaCl(aq) and CO_2; □, MD of $CaCl_2$(aq) and CO_2; and ●, ref 15.

at 373 K. First, we observe that for the TIP4P water model the IFTs of brine and CO_2 increase linearly with increasing salt concentration. Second, for different types of ions, the IFT is found to increase linearly with positive charge concentration regardless of the type of ions.

From the Gibbs adsorption isotherm for multicomponent systems, the concentration of ions, CO_2, and water within the interface are related to the IFT. The Gibbs adsorption equation in terms of surface excess can be written as

$$-d\gamma = \Gamma_{water} d\mu_{water} + \Gamma_{CO_2} d\mu_{CO_2} + \Gamma_{ion} d\mu_{ion} \quad (3)$$

where γ is the IFT, Γ is the interfacial excess, and μ is the chemical potential.

This equation indicates that when the surface excess of a component is positive, increasing the chemical potential of that

dx.doi.org/10.1021/jp309730m | J. Phys. Chem. B 2013, 117, 5647−5652

component reduces the IFT; when the surface excess of a component is negative, increasing the chemical potential of that component increases the IFT. In the system of CO_2 and brine, an arbitrary reference plain where $\Gamma^0_{water} = 0$ can be found with in the interface zone. Thus the term $\Gamma_{water}\, d\mu_{water} = 0$, and eq 3 can be written as

$$-d\gamma = \Gamma^0_{CO_2} d\mu_{CO_2} + \Gamma^0_{ion} d\mu_{ion} \quad (4)$$

As previously discussed, the MD simulation shows that $\Gamma^0_{CO2} > 0$, and $\Gamma^0_{ion} < 0$. In a process of increasing the concentration of salt in brine, but maintain the temperature and pressure, the chemical potential of the ions increases, from which term $\Gamma^0_{ion}\, d\mu_{ion} < 0$. However the solubility of CO_2 decreases as a salting out effect occurred, also resulting in a contribution $\Gamma^0_{ion}\, d\mu_{ion} < 0$. From eq 4, it can be concluded that the IFT of the brine and CO_2 system decreases with increasing salt concentration.

3.4. Solubility. Molecular dynamics simulations also predict the solubility of CO_2 in brine and the mole fraction of water vapor in CO_2 (Figures 12 and 13). The solubility of CO_2 in

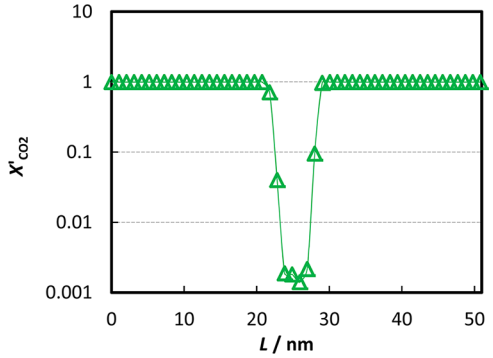

Figure 12. Solubility of CO_2 in pure water (no salt)−CO_2 system at T = 373 K, p = 2 MPa. Particle numbers: Ca^{2+}, 128; Cl^-, 256; water TIP4P, 4096; and CO_2 EPM2, 512.

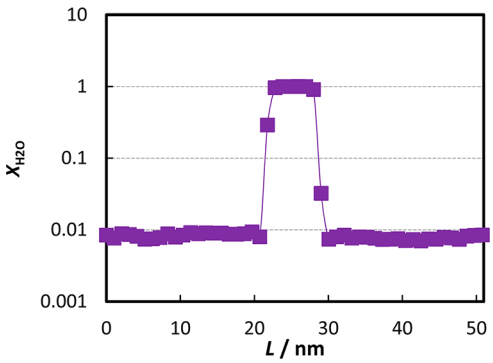

Figure 13. Solubility of water in CO_2 $CaCl_2$(aq)−CO_2 system at T = 373 K, p = 2 MPa. Particle numbers: Ca^{2+}, 128; Cl^-, 256; water TIP4P, 4096; and CO_2 EPM2m, 512.

pure water (no salt) at 373 K and 2 MPa from our MD simulation is 0.0018 ± 0.0005, in excellent agreement with the reference value of 0.0021 from Duan's model.[37] The mole fraction of water vapor under the same condition from our MD simulation is 0.008 ± 0.001, while the reference value from SAFT calculations is 0.050 ± 0.005. We suggest that the smaller value obtained from the MD simulations may be due to equilibration issues or because the system size is too small. We expect that Gibbs ensemble calculations may give improved results to estimate such concentrations. This will be a topic for our future research.

4. CONCLUSIONS

In this work, molecular dynamics simulations have been performed to study the IFT of CO_2 and brine for a range of temperatures between 303 and 393 K and pressures from 2 to 50 MPa. The ions involved in this study are Na^+, Ca^{2+}, and Cl^-. The results indicate that the IFT decreases with increasing pressure under any temperature condition but increases linearly with the molality of the salt solution. We generally observe good qualitative agreement between experimental and simulation IFT data. However, quantitatively the simulation data start to deviate from the experiment with pressure increasing. To check this point, we calculated the brine density with pressure increasing. We observe that the simulated brine density follows the same trend as the experimental correlation for both SPC/E and TIP4P water. Therefore, we suggest that the deviation in IFT is not due to density deviation but may be due to other simulation parameters such as system size. Alternatively the rigid molecular structures for water used in the MD simulation may not be sensitive enough at higher pressures. We will report on a detailed analysis of such effects in a forthcoming paper. For the first time we calculated density profiles from the MD simulation for a CO_2 and brine system. The results indicate a positive excess of CO_2 and a negative excess of ions at the interface. The charge of the ions was found to have a larger influence than their size on the IFT, a result that is consistent with experimental findings.

AUTHOR INFORMATION

Corresponding Author

*E-mail: e.boek@imperial.ac.uk.

Notes

The authors declare no competing financial interest.

ACKNOWLEDGMENTS

This work was carried out as part of the activities of the Qatar Carbonates & Carbon Storage Research Centre (QCCSRC). We gratefully acknowledge the funding of QCCSRC provided jointly by Qatar Petroleum, Shell, and the Qatar Science and Technology Park, and their permission to publish this research. We are grateful to one anonymous referee and S. Al Ghafri for useful suggestions.

REFERENCES

(1) Shedid, A, S. Influences of Fracture Orientation on Oil Recovery by Water and Polymer Flooding Processes: An Experimental Approach. *J. Pet. Sci. Eng.* **2006**, *50*, 285−292.

(2) Blunt, M.; Fayers, F. J.; Orr, F. M., Jr. Carbon Dioxide in Enhanced Oil Recovery. *Energy Convers. Manage.* **1993**, *34*, 1197−1204.

(3) Rogers, J. D.; Grigg, R. B. a Literature Analysis of the WAG Injectivity Abnormalities in the CO_2 Process. *SPE Reservoir Eval. Eng.* **2001**, *4*, 375−386.

(4) Blom, S. M. P.; Hagoort, J.; Soetekouw, D. P. N. Relative Permeability at near-Critical Conditions. *SPE J.* **2000**, *5*, 172−181.

(5) Blom, S. M. P.; Hagoort, J. The Combined Effect of Near-Critical Relative Permeability and Non-Darcy Flow on Well Impairment by Condensate Drop Out. *SPE Reservoir Eval. Eng.* **1998**, *1*, 421−429.

(6) Grattoni, C. A.; Jing, X. D.; Dawe, R. A. Dimensionless Groups for Three-Phase Gravity Drainage Flow in Porous Media. *J. Pet. Sci. Eng.* **2001**, *29*, 53−65.

(7) Bennion, D. B.; Bachu, S., The Impact of Interfacial Tension and Pore Size Distribution/Capillary Pressure Character on CO_2 Relative Permeability at Reservoir Conditions in CO_2-Brine Systems. In *SPE/DOE Symposium on Improved Oil Recovery*, Tulsa, OK, 2006.
(8) Bachu, S.; Bennion, B. Effects of in-Situ Conditions on Relative Permeability Characteristics of CO_2-Brine systems. *Environ. Geol.* **2008**, *54*, 1707−1722.
(9) Jaeger, P. T.; Alotaibi, M. B.; Nasr-El-Din, H. A. Influence of Compressed Carbon Dioxide on the Capillarity of the Gas−Crude Oil−Reservoir Water System. *J. Chem. Eng. Data* **2010**, *55*, 5246−5251.
(10) Karimaie, H.; Torsæter, O. Low IFT Gas-Oil Gravity Drainage in Fractured Carbonate Porous Media. *J. Pet. Sci. Eng.* **2010**, *70*, 67−73.
(11) Sun, C.-Y.; Chen, G.-J. Measurement of Interfacial Tension for the CO_2 Injected Crude Oil + Reservoir Water System. *J. Chem. Eng. Data* **2005**, *50*, 936−938.
(12) Yang, D. Y.; Tontiwachwuthikul, P.; Gu, Y. G. Dynamic Interfacial Tension Method for Measuring Gas Diffusion Coefficient and Interface Mass Transfer Coefficient in a Liquid. *Ind. Eng. Chem. Res.* **2006**, *45*, 4999−5008.
(13) Yang, D.; Tontiwachwuthikul, P.; Gu, Y. Interfacial Tensions of the Crude Oil + Reservoir Brine + CO_2 Systems at Pressures up to 31 MPa and Temperatures of 27 and 58 °C. *J. Chem. Eng. Data* **2005**, *50*, 1242−1249.
(14) Jarrell, P. M.; Fox, C. E.; Stein, M. H.; Webb, S. L. *Practical Aspects of CO_2 flooding*; Society of Petroleum Engineers: Dallas, 2002; Vol. *22*.
(15) Li, X.; Boek, E. S.; Maitland, G. C.; Trusler, J. P. M. Interfacial Tension of (Brines + CO_2): $CaCl_2$(aq), $MgCl_2$(aq), and Na_2SO_4(aq) at Temperatures between (343 and 423) K, Pressures between (2 and 50) MPa, and Molalities of (0.5 to 5) mol·kg^{-1}. *J. Chem. Eng. Data* **2012**, *57*, 1369−1375.
(16) Li, X.; Boek, E.; Maitland, G. C.; Trusler, J. P. M. Interfacial Tension of (Brines + CO_2): (0.864 NaCl + 0.136 KCl) at Temperatures between (298 and 448) K, Pressures between (2 and 50) MPa, and Total Molalities of (1 to 5) mol·kg^{-1}. *J. Chem. Eng. Data* **2012**, *57*, 1078−1088.
(17) M. In Het Panhuis, C. H.; Patterson, R. M, L.-B. a Molecular Dynamics Study of Carbon Dioxide in Water: Diffusion, Structure and Thermodynamics. *Mol. Phys.* **1998**, *94*, 963−972.
(18) da Rocha, S. R. P.; Johnston, K. P.; Westacott, R. E.; Rossky, P. J. Molecular Structure of the Water−Supercritical CO_2 Interface. *J. Phys. Chem. B* **2001**, *105*, 12092−12104.
(19) Zhang, Z.; Duan, Z. An Optimized Molecular Potential for Carbon Dioxide. *J. Chem. Phys.* **2005**, *122*, 214507−214515.
(20) Kvamme, B.; Kuznetsova, T.; Hebach, A.; Oberhof, A.; Lunde, E. Measurements and Modelling of Interfacial Tension for Water + Carbon Dioxide Systems at Elevated Pressures. *Comput. Mater. Sci.* **2007**, *38*, 506−513.
(21) Nieto-Draghi, C.; de Bruin, T.; Perez-Pellitero, J.; Avalos, J. B.; Mackie, A. D. Thermodynamic and Transport Properties of Carbon Dioxide from Molecular Simulation. *J. Chem. Phys.* **2007**, *126*, 064509−8.
(22) Chen, F. Simulated Surface Tensions of Common Water Models. *J. Chem. Phys.* **2007**, *126*, 221101.
(23) Nielsen, L. C.; Bourg, I. C.; Sposito, G. Predicting CO_2−water Interfacial Tension under Pressure and Temperature Conditions of Geologic CO_2 Storage. *Geochim. Cosmochim. Acta* **2012**, *81*, 28−38.
(24) Berendsen, H. J. C.; Grigera, J. R.; Straatsma, T. P. The Missing Term in Effective Pair Potentials. *J. Phys. Chem.* **1987**, *91*, 6269−6271.
(25) Abascal, J. L. F.; Vega, C. a General Purpose Model for the Condensed Phases of Water: TIP4P/2005. *J. Chem. Phys.* **2005**, *123*, 234505−12.
(26) Harris, J. G.; Yung, K. H. Carbon Dioxide's Liquid-Vapor Coexistence Curve And Critical Properties as Predicted by a Simple Molecular Model. *J. Phys. Chem.* **1995**, *99*, 12021−12024.
(27) Tegze, G.; Pusztai, T.; Toth, G.; Granasy, L.; Svandal, A.; Buanes, T.; Kuznetsova, T.; Kvamme, B. Multiscale Approach to CO_2 Hydrate Formation in Aqueous Solution: Phase Field Theory and Molecular Dynamics. Nucleation and Growth. *J. Chem. Phys.* **2006**, *124*, 234710−12.
(28) Alejandre, J.; Tildesley, D. J.; Chapela, G. A. Molecular Dynamics Simulation of the Orthobaric Densities and Surface Tension of Water. *J. Chem. Phys.* **1995**, *102*, 4574−4583.
(29) Wasserman, E.; Wood, B.; Brodhol, J. the Static Dielectric Constant of Water at Pressures up to 20 kbar and Temperatures to 1273 K: Experiment, Simulations, and Empirical Equations. *Geochim. Cosmochim. Acta* **1995**, *59*, 1−6.
(30) Duan, Z.; Zhang, Z. Equation of State of the H_2O, CO_2, and H_2O−CO_2 Systems up to 10 GPa and 2573.15 K: Molecular Dynamics Simulations with Ab Initio Potential Surface. *Geochim. Cosmochim. Acta* **2006**, *70*, 2311−2324.
(31) Vega, C.; de Miguel, E. Surface Tension of the Most Popular Models of Water by Using the Test-Area Simulation Method. *J. Chem. Phys.* **2007**, *126*, 154707−10.
(32) Jorgensen, W. L.; Maxwell, D. S.; Tirado-Rives, J. Development and Testing of the OPLS All-Atom Force Field on Conformational Energetics and Properties of Organic Liquids. *J. Am. Chem. Soc.* **1996**, *118*, 11225−11236.
(33) Hess, B.; Kutzner, C.; van der Spoel, D.; Lindahl, E. GROMACS 4: Algorithms for Highly Efficient, Load-Balanced, and Scalable Molecular Simulation. *J. Chem. Theory Comp.* **2008**, *4*, 435−447.
(34) Lemmon, E.; Huber, M. L.; McLinden, M. O. *NIST Standard Reference Database 23: Reference Fluid Thermodynamic and Transport Properties - REFPROP*; NIST: Gaithersburg, MD, 2010.
(35) Georgiadis, A.; Maitland, G.; Trusler, J. P. M.; Bismarck, A. Interfacial Tension Measurements of the (H_2O + CO_2) System at Elevated Pressures and Temperatures. *J. Chem. Eng. Data* **2010**, *55*, 4168−4175.
(36) Harris, J. G. Liquid-Vapor Interfaces of Alkane Oligomers: Structure and Thermodynamics from Molecular Dynamics Simulations of Chemically Realistic Models. *J. Phys. Chem.* **1992**, *96*, 5077−5086.
(37) Duan, Z.; Sun, R. An Improved Model Calculating CO_2 Solubility in Pure Water and Aqueous NaCl Solutions from 273 to 533 K and from 0 to 2000 bar. *Chem. Geol.* **2003**, *193*, 257−271.
(38) Zhao, L.; Lin, S.; Mendenhall, J. D.; Yuet, P. K.; Blankschtein, D. *J. Phys. Chem. B* **2011**, *115*, 6076−6087.
(39) Watanabe, K.; Okajima, H.; Kato, T.; Hamaguchi, H. *J. Chem. Phys.* **2012**, *136*, 014508.
(40) Al Ghafri, S.; Maitland, G. C.; Trusler, J. P. M. *J. Chem. Eng. Data* **2012**, *57*, 1288−1304.